Bioactivation Pathways of the CB1r Antagonist Rimonabant

Moa Andresen Bergström, Emre M. Isin, Neal Castagnoli Jr., and Claire E. Milne

CVGI iMED DMPK, AstraZeneca R&D Mölndal, Sweden (M.A.B., E.M.I., C.E.M.); Department of Chemistry, Virginia Tech, and Virginia College of Osteopathic Medicine, Blacksburg, VA 24061 (N.C.)

DMD Fast Forward. Published on July 6, 2011 as DOI: 10.1124/dmd.111.039412
This article has not been copyedited and formatted. The final version may differ from this version.

Running Title: Bioactivation Pathways of the CB1r Antagonist Rimonabant

Corresponding Author: Dr. Moa Andresen Bergström, CVGI iMED DMPK, AstraZeneca R&D Mölndal, SE-431 83 Mölndal, Sweden.

Tel.: +46317762551, Fax.: +46317763760,

E-mail: moa.andresen.bergstrom@astrazeneca.com.

Number of Text Pages: 18

Number of Tables: 2

Number of Figures: 6

Number of Schemes: 3

Number of References: 40

Number of Words in Abstract: 227

Number of Words in Introduction: 604

Number of Words in Discussion: 1500

List of Nonstandard Abbreviations: ADRs, adverse drug reactions; BFC, 7-benzyloxy-4-trifluoromethylcoumarin; CYP, cytochrome P450; HFC, 7-hydroxy-4-(trifluoromethyl)coumarin; HLMs, human liver microsomes; IADRs, idiosyncratic adverse drug reactions; KCN, potassium cyanide; LC, liquid chromatography; LSC, liquid scintillation counting; MS, mass spectrometry; RAD, radiochemical detection; RLMs, rat liver microsomes; TDI, time-dependent inhibition

Abstract

In the present work, the characterization of the biotransformation and bioactivation pathways of the cannabinoid receptor 1 antagonist rimonabant (Acomplia®) is described. Rimonabant was approved in Europe in 2006 for the treatment of obesity but was withdrawn in 2008 due to a significant drug-related risk of serious psychiatric disorders. The aim of the present work is to characterize the biotransformation and potential bioactivation pathways of rimonabant in vitro in human and rat liver microsomes. The observation of a major iminium ion metabolite led us to perform reactive metabolite trapping, covalent binding to proteins and time-dependent inhibition of cytochrome P450 3A4 studies. The major biotransformation pathways were oxidative dehydrogenation of the piperidinyl ring to an iminium ion, hydroxylation of the 3-position of the piperidinyl ring and cleavage of the amide linkage. In co-incubations with potassium cyanide, three cyanide adducts were detected. A high level of covalent binding of rimonabant in human liver microsomes was observed (920 pmol eq./mg protein). In co-incubations with potassium cyanide and methoxylamine, the covalent binding was reduced by ca 40% and 30%, respectively whereas GSH had no significant effect on covalent binding levels. Rimonabant was also found to inhibit cytochrome P450 3A4 irreversibly in a time dependent manner. In view of these findings it is noteworthy that, to date, no toxicity findings related to the formation of reactive metabolites from rimonabant have been reported.

DMD Fast Forward. Published on July 6, 2011 as DOI: 10.1124/dmd.111.039412
This article has not been copyedited and formatted. The final version may differ from this version.

Introduction

Introduction

Rimonabant (Acomplia®, Figure 1) is an *N*-acylaminopiperidinyl derivative with CB1r antagonist properties that has been reported to be effective in appetite control and smoking cessation therapy (Boyd and Fremming, 2005). CB1r and CB2r are G-protein coupled receptors that are expressed in mammalian tissues as part of the endocannabinoid system (Howlett et al., 2004; Pertwee, 2006). In humans, CB1r is mainly expressed in the brain whereas CB2r expression is concentrated in the major tissues of the immune system including spleen, tonsils and thymus (Howlett et al., 2002). Cannabinoid receptor activation in the brain is involved in a variety of cellular signaling pathways (Dalton et al., 2009). Both antagonists and agonists of CB1r receptors have been evaluated as potential drug candidates (Di Marzo, 2009). Rimonabant was the first CB1r antagonist to be approved for the treatment of obesity in Europe (Van Gaal et al., 2005; Henness et al., 2006). It was withdrawn from the market in 2008 as it was found to cause a significant drug-related risk of serious psychiatric disorders including anxiety and depression (Christensen et al., 2007). Since an understanding of the metabolic fate of rimonabant should be useful in our drug design efforts, we have pursued studies to characterize the in vitro biotransformation pathways of this compound with special emphasis on the potential formation of chemically reactive metabolites.

Formation of reactive metabolites and their covalent interactions with proteins have been proposed to be involved in adverse drug reactions (ADRs) including idiosyncratic ADRs (IADRs) (Guengerich and MacDonald, 2007; Uetrecht, 2008). IADRs are severe but so rare that they often are detected only after a large patient population has been exposed to the drug. This problem is further complicated by the limited value of preclinical safety models (Shenton et al., 2004). Biotransformation pathways leading to reactive metabolites have been

documented via metabolite identification and chemical trapping studies (Kalgutkar and Soglia, 2005). It has been proposed that potential toxicological outcomes may also be predicted by estimating the extent of metabolism-dependent covalent binding to proteins (Evans et al., 2004; Bauman et al., 2009; Nakayama et al., 2009). However, the structural features of the drug-protein adducts and the down-stream processes leading to adverse drug reactions are not well-understood.

Iminium ion formation via metabolic ring α-carbon oxidation of cyclic tertiary amines such as rimonabant has been reported for a variety of drugs including phencyclidine (Owens et al., 1993), nicotine (Murphy, 1973; Shigenaga et al., 1988), haloperidol (Avent et al., 2006), ticlopidine (Dalvie and O'Connell, 2004) and 1-methyl-4-phenyl-1,2,3,6-tetrahydropyridine (MPTP) (Castagnoli et al., 1997). Iminium ion metabolites are electrophilic and have in some cases been linked to covalent binding to proteins. Examples include phencyclidine (Ward et al., 1982), nicotine (Obach and Van Vunakis, 1988; Shigenaga et al., 1988) and a dihydrobenzoxathiin analogue (Zhang et al., 2005b). These metabolites have been characterized both directly and via the corresponding α-cyanoamines that are formed in incubation mixtures containing potassium cyanide (KCN). Inhibition of metabolism-dependent covalent binding of drugs to proteins by KCN has also been observed (Ward et al., 1982, Baillie, 2008), and is consistent with the potential contribution of iminium ion metabolites to drug-mediated toxicities. Furthermore, cyclic iminium ions are in equilibrium with the corresponding carbinolamines, enamines and potentially reactive aminoaldehydes (Scheme 1) (Sayre et al., 1997; Masic, 2011). The extent to which aminoaldehydes versus the iminium species contribute to covalent binding is yet to be determined.

DMD Fast Forward. Published on July 6, 2011 as DOI: 10.1124/dmd.111.039412
This article has not been copyedited and formatted. The final version may differ from this version.

The aim of the present work is to characterize the biotransformation and potential bioactivation pathways of rimonabant in vitro in human and rat liver microsomes (HLMs and RLMs). The observation of a major iminium ion metabolite led us to perform reactive metabolite trapping, covalent binding to proteins and time-dependent inhibition of cytochrome P450 (CYP) 3A4 studies.

Methods

Chemicals and Biochemicals. [^{14}C]Rimonabant was provided by Isotope Chemistry, AstraZeneca R&D, Mölndal and had a radiochemical purity of >99% and a specific activity of 2.67 kBq/nmol. *N*-Aminopiperidine and unlabelled rimonabant were supplied by Compound Management, AstraZeneca R&D. HLMs (20 mg protein/mL, pooled, >10 donors, male and female) and 7-benzyloxy-4-trifluoromethylcoumarin (BFC) were obtained from Gentest (BD Biosciences, Woburn, MA). RLMs (20 mg protein/mL, pooled, female) were purchased from Cellzdirect (Austin, TX). Recombinant CYP3A4 expressed in *E. coli* used for TDI experiments was purchased from Cypex (Dundee, UK). Recombinant CYP3A4 expressed in yeast used in the potassium ferricyanide displacement experiments was obtained from AstraZeneca Biotech Lab (Södertälje, Sweden). Reduced NADPH, reduced L-glutathione (GSH), methoxylamine hydrochloride, potassium ferricyanide, troleandomycin and betamethasone were purchased from Sigma-Aldrich (St. Louis, MO). Potassium cyanide (KCN) was obtained from Acros Organics (Geel, Belgium). The scintillation cocktail for liquid scintillation counting (LSC) was OptiPhase 'Hisafe' 3 (PerkinElmer, Boston, MA). All other chemicals were obtained from commercial sources.

DMD Fast Forward. Published on July 6, 2011 as DOI: 10.1124/dmd.111.039412
This article has not been copyedited and formatted. The final version may differ from this version.

Liver microsomal incubations. [^{14}C]Rimonabant (10 μM, 2.67 kBq/nmol) was incubated with HLMs or RLMs (1 mg protein/mL) in the presence of NADPH (1 mM) and $MgCl_2$ (5 mM) in potassium phosphate buffer (0.1 M, pH 7.4) in a total volume of 500 μL. Incubations in the absence of NADPH served as negative control. The HLM incubations carried out in the presence of a trapping agent contained either KCN (1 mM), GSH (5 mM) or methoxylamine (5 mM). The reactions were initiated by the addition of NADPH following a 3 min pre-incubation period at 37°C. The incubations were terminated after 60 min and the protein was precipitated by the addition of 1 mL ice-cold methanol. The samples were placed on ice for 10 min and then centrifuged at 3000*g* and 4°C for 15 min. The supernatants were stored at -20°C until analyzed.

LC-MS-RAD analysis of HLM incubations. The supernatants from the incubations were analyzed using liquid chromatography (LC) combined with radioactivity detection (RAD) for quantification, and mass spectrometry (MS) for structural elucidation of parent compound and metabolites.

The LC system (Agilent Series 1100, Palo Alto, CA) consisted of an autosampler, a solvent degassing unit and a gradient pump. The column oven was set to 25°C and sample tray temperature to 8°C. The mobile phases used were A: H_2O containing 0.1% formic acid and B: acetonitrile. Chromatographic separations were performed on an Eclipse XDB-C8 LC column (4.6 mm i.d. x 150 mm; particle size 5 μm) protected by an Optiguard CN column (1 mm i.d.). A flow rate of 1 mL/min was used. A post-column split directed 0.1 mL/min of the flow into the mass spectrometer and the remaining 0.9 mL/min flow was transferred for fraction collection into Deep-Well LumaPlate Microplates (Packard Instrument Co., Meriden, CT) using a Gilson FC204 fraction collector (Gilson Inc., Middleton, WI) and a collection time of

0.16 min/well. All samples were diluted with two equivalents of water before analysis and the injection volume was 40 μL. The following LC gradient was used for the analysis of rimonabant incubations: The gradient program started with a 20 min linear gradient from 40% B to 60% B that was followed with 5 min of isocratic elution at 60% B. The column was then washed with 95% B for 3.5 min whereafter the eluent composition returned to the initial conditions (40% B) for 5.5 min. The total run time was 34 min.

The mass detector used was a high mass accuracy hybrid quadrupole time of flight mass spectrometer (Waters Micromass Q-Tof 2, Milford, MA) with an electrospray interface (ESI) and a LockSpray^{TM} probe. Specific mass spectrometric source conditions were: cone voltage 40 V, capillary voltage 3.20 kV, MCP 2000 V, TOF 9.10 kV, source temperature 120°C and desolvation temperature 320°C. MassLynx (version 4, Waters) was used for controlling the mass spectrometer and for data evaluation. The mass range was *m/z* 80 to 1000 and MS spectra were acquired in the positive ionization mode. MSMS spectra were acquired on the most abundant isotope (containing two ^{14}C labels) of the molecular ion cluster using a mass window of 1 Da. The collision energies used ranged between 15 to 25 V and the mass range for the product ions was *m/z* 80 to 650. MS^3 data for **M3** and **CA2** was obtained by raising the cone voltage to 45-55 V and selecting the *m/z* 465 in source fragment ions for MSMS analysis.

The microplates containing the collected fractions were allowed to dry in a ventilated area at room temperature and were then closed with sealing film (TopSeal A, Packard Instrument Co.) and placed in a microplate scintillation counter (TopCount, Packard Instrument Co.) with 12 detectors. The microplates were counted for 4 mins per well. The counting results were

DMD Fast Forward. Published on July 6, 2011 as DOI: 10.1124/dmd.111.039412
This article has not been copyedited and formatted. The final version may differ from this version.

analyzed and radiochromatograms integrated using Laura (version 3, LabLogic, Sheffield, UK).

Covalent binding to HLM proteins

The precipitated protein pellets from the HLM incubations were washed with methanol (2 x 1 mL), acetonitrile (2 x 1 mL) and acetonitrile/water (4:1, 2 x 1 mL). The pellets were disintegrated by vortex mixing and the washing solvent was removed to waste after centrifugation at ca 3000*g* and 4°C for 10 min. After the sixth wash, 200 μL aliquots of the washing solvent were mixed with 5 mL of scintillation cocktail and analyzed using LSC on a Wallac 1409 instrument (Wallac Oy, Kuopio, Finland) to ensure that the pellets had been adequately washed. Each pellet was dissolved by warming in 1 mL 0.1 M aqueous sodium hydroxide containing 5% sodium dodecyl sulfate at 40°C over night in a shaking water bath. The resulting solutions were analyzed for total radioactivity using static LSC and the protein content was determined using the Markwell-modified Lowry assay with bovine serum albumin as standard (Markwell et al., 1978). The radioactive concentration in the protein solutions was determined by analyzing each sample in triplicate by LSC. Aliquots of protein solution (250 μL) were mixed with OptiPhase 'Hisafe' 3 scintillation liquid (15 mL) in 20 mL glass scintillation vials. Each sample was counted for 10 min or until the variance was ≤1% using a protocol with automatic subtraction of background activity and quench curve correction. The levels of binding indicated by non-extractable radioactivity were expressed as pmol equivalents per milligram protein (pmol eq./mg protein) using the specific activity of the test compound and the protein levels for each sample, according to the following equation:

$$\text{Amount of binding (pmol eq./mg protein)} = \frac{\text{Measured radioactive concentration (Bq/mL)}}{\text{Specific activity (Bq/pmol)} \times \text{Protein concentration (mg/mL)}}$$

DMD Fast Forward. Published on July 6, 2011 as DOI: 10.1124/dmd.111.039412
This article has not been copyedited and formatted. The final version may differ from this version.

Time-dependent inhibition of CYP3A4. The assay was performed in two steps. In the first step, rimonabant (1 μM) was incubated with CYP3A4 (50 nM) in potassium phosphate buffer (0.2 M, pH 7.4) in the presence or absence of NADPH (1 mM) at 37°C for 10 mins. The incubations were performed in dublicates and the total incubation volume was 100 μL. In the second step, an aliquot (10 μL) from each incubation was transferred to a prewarmed plate which contained buffer and BFC (20 μM). The reaction was started by addition of NADPH (1 mM) and the plate was incubated at 37°C for 15 mins. The total incubation volume was 200 μL. The incubations were stopped by addition of 75 μL of acetonitrile and 0.5 M Tris-Base (8:2 v/v). The conversion of BFC to 7-hydroxy-4-(trifluoromethyl)coumarin (HFC) was measured by fluorescence spectroscopy (excitation wavelength 405 nm, emission wavelength 535 nm). Troleandomycin (0.1 μM) and betamethasone (5 μM) were used as positive and negative controls, respectively. The time dependent inhibition of CYP3A4 was calculated as a normalized ratio, according to the following equation:

$$\text{Normalized ratio} = \frac{F^{+I+NADPH} / F^{-I+NADPH}}{F^{+I-NADPH} / F^{-I-NADPH}}$$

$F^{+I+NADPH}$ is the fluorescence intensity measured for the reaction performed with inhibitor and NADPH

$F^{-I+NADPH}$ is the fluorescence intensity measured for the reaction performed with NADPH and without inhibitor

$F^{+I-NADPH}$ is the fluorescence intensity measured for the reaction performed with inhibitor and without NADPH

$F^{-I-NADPH}$ is the fluorescence intensity measured for the reaction performed without inhibitor and NADPH

Displacement study with potassium ferricyanide. The assay was performed in three steps. In the first step, the test compound (5 μM) was incubated with CYP3A4 (200 nM) in potassium phosphate buffer (0.2 M, pH 7.4) in the presence or absence of NADPH (1 mM) at 37°C for 45 mins. The total incubation volume was 200 μL. In the second step, an aliquot from each incubation (50 μL) was added to either potassium ferricyanide in phosphate buffer (50 μL, 2 mM) or potassium phosphate buffer alone (50 μL). The mixtures were incubated at 37°C for 15 mins. In the third step, an aliquot from each potassium ferricyanide incubation

DMD Fast Forward. Published on July 6, 2011 as DOI: 10.1124/dmd.111.039412
This article has not been copyedited and formatted. The final version may differ from this version.

(10 μL) was transferred to a plate which contained potassium phosphate buffer and BFC (13 μM). The reactions were started by the addition of NADPH (1 mM) and the plate was incubated at 37°C for 30 mins. The total incubation volume was 200 μL. The incubations were stopped by addition of 75 μL of acetonitrile and 0.5 M Tris-Base (8:2 v/v). The conversion of BFC to HFC was measured by fluorescence spectroscopy (excitation wavelength 405 nm, emission wavelength 535 nm). The time dependent inhibition of CYP3A4 was calculated as a normalized ratio, using the equation in the above section. Troleandomycin (20 μM) was used as a positive control for potassium ferricyanide-reversible TDI.

Results

Metabolite profiling and metabolite identification in HLMs and RLMs. The supernatants from the liver microsomal incubations were analyzed by LC-MS-RAD for structural elucidation and quantification of metabolites and trapped intermediates. Quantitative estimates and radiochemical metabolite profiles are shown in Table 1 and Figure 2, respectively. The metabolite pathways of rimonabant in HLMs and cyanide trapping results are summarized in Scheme 2. Metabolites (**M**) are numbered in order of retention time. The major metabolites detected in HLMs in the presence of NADPH were **M1** (not detectable by MS), **M3** (+16 Da) and **M7** (–2 Da). Using a synthetic standard, the early eluting metabolite **M1** was identified as the amide hydrolysis product *N*-aminopiperidine (Scheme 2). The carboxylic acid moiety formed via the amide hydrolysis reaction was detected by MS at *m/z* 381.00 (LC retention time 17.0 min). This metabolite is denoted **M9** and was not quantified since it has lost the ^{14}C label. Minor metabolites detected were **M6** (+16 Da) and **M2**, **M4**, **M5** and **M8** (all +14 Da). Similar to the HLM incubations, the major metabolites formed in RLMs were **M1**, **M3** and **M7**. The minor metabolite **M6** (+16 Da) was also identified in

DMD Fast Forward. Published on July 6, 2011 as DOI: 10.1124/dmd.111.039412
This article has not been copyedited and formatted. The final version may differ from this version.

RLMs but no +14 Da metabolites were detected. Trace amounts of metabolites **M1** and **M7** were detected in the incubations run in the absence of NADPH.

Metabolite identification in the presence of trapping agents. To investigate the formation of reactive metabolites, HLM incubations were carried out with [^{14}C]rimonabant in the presence of the following trapping agents: GSH, KCN and methoxylamine. The incubation mixtures were analyzed using LC-MS-RAD. GSH is known to be a broad and efficient reactive metabolite scavenger whereas KCN and methoxylamine are more selective trapping agents and are used to trap reactive iminium ions and aldehydes, respectively (Evans et al., 2004; Argoti et al., 2005).

No adducts were detected in the incubations containing GSH or methoxylamine and the metabolite profiles from these incubations were similar to that observed in the absence of trapping agent. In the incubations with KCN, three cyanide adducts were detected and denoted **CA1**, **CA2** and **CA3** in order of retention time (Figure 1 and Table 1). The molecular ions observed of **CA1**, **CA2** and **CA3** were 41, 25 and 23 Da higher, respectively, than the mass of rimonabant. Thus, **CA1** corresponds to a monooxygenated cyanide adduct, **CA2** to an otherwise unmodified cyanide adduct and **CA3** to a dehydrogenated cyanide adduct. Furthermore, metabolites **M2** and **M4** (+14 Da) were absent and the amount of **M7** (-2 Da) was almost depleted in the incubations containing cyanide. It is plausible that **CA1** is formed from **M2** and/or **M4** and **CA2** from **M7**. No -4 Da metabolite, which could account for the formation of **CA3**, was detected in the incubations performed in the absence of cyanide. However, it is possible that this metabolite is a short-lived intermediate or that **CA3** is formed via further oxidative dehydrogenation of **CA2**.

DMD Fast Forward. Published on July 6, 2011 as DOI: 10.1124/dmd.111.039412
This article has not been copyedited and formatted. The final version may differ from this version.

Covalent binding in HLMs. Based on the observation of KCN-trappable reactive iminiumyl metabolites in the HLM incubations, the extent of covalent binding of rimonabant to microsomal proteins in the HLM incubations was assessed (Table 2 and Figure 3). A high degree of binding (920 pmol drug eq./mg protein) was observed in incubations in the presence of NADPH. This corresponds to binding of ca 19% of the metabolites formed from rimonabant (a fraction covalent binding of 0.19). Low levels of background binding (10 pmol drug eq./mg protein) were observed in the incubations run in the absence of NADPH. To gain insight into the nature of the reactive metabolites responsible, covalent binding to proteins in the co-incubations with the reactive metabolite trapping agents was also measured (Table 2 and Figure 3). The covalent binding values were normalized for total metabolic conversion of rimonabant (measured by LC-RAD) with respect to the incubations in the presence of NADPH. This way, the changes in covalent binding attributable to the differences in turnover among different incubations are accounted for. Only a marginal reduction of binding was observed in the incubations with GSH. However, both KCN and methoxylamine gave rise to significant reductions of covalent binding of rimonabant to HLM proteins, with KCN (40% reduction) being more efficient than methoxylamine (30% reduction). The addition of KCN and GSH to the incubations had no major effects on the metabolic turnover of rimonabant, whereas methoxylamine significantly inhibited the metabolism (Table 2).

Time-dependent inhibition (TDI) of CYP3A4. A TDI experiment with rimonabant and CYP3A4 was carried out to investigate if the observed covalent binding could lead to enzyme inactivation. The major metabolic pathway of rimonabant is reported to be mediated by CYP3A4 (EMEA, 2006). Therefore the possible metabolism-dependent inhibition of this enzyme was considered relevant to our study. After pre-incubation of CYP3A4 in the presence or absence of rimonabant, the incubation mixture was diluted 20-fold and BFC, a

known CYP3A4 substrate, was added. A reduction of BFC metabolism in incubations with NADPH in the presence of inhibitor compared to the absence of inhibitor is considered as an indicator of TDI. For the rimonabant incubations performed at 5 μM, clear evidence of TDI was observed as the BFC metabolism was inhibited by ca 70% (Figure 4 and Supplementary Figure 1). Troleandomycin and betametazone were included as positive and negative controls (Atkinson et al., 2005; Grimm et al., 2009).

To further investigate the mechanism of the observed TDI with rimonabant, a potassium ferricyanide oxidative reactivation experiment was performed. In this experiment, an extra incubation step with potassium ferricyanide between the rimonabant incubation and the BFC incubation is conducted. Co-incubation with potassium ferricyanide is used to determine if the inhibition is irreversible (mechanism-based inhibition caused by covalent modification) or quasi-irreversible (caused by non-covalent interactions) (Polasek and Miners, 2007; Riley et al., 2007). The potassium ferricyanide oxidizes the heme iron and results in the displacement of non-covalently bound high affinity inhibitors coordinating the ferrous state of heme iron, such as troleandomycin, and results in reactivation of the enzyme (Franklin, 1991). This reversibility is not observed for covalently bound inhibitors (Polasek and Miners, 2007; Riley et al., 2007). Potassium ferricyanide treatment did not lead to an increase in metabolism of BFC in rimonabant incubations (Figure 5) but, as expected, did lead to an increase in the metabolism of BFC in troleandomycin incubations. Therefore the TDI observed for rimonabant is most likely due to mechanism-based inhibition of CYP3A4.

Discussion

Since an understanding of the metabolic fate of rimonabant should be useful in our drug design efforts, we have characterized the in vitro biotransformation pathways of this

DMD Fast Forward. Published on July 6, 2011 as DOI: 10.1124/dmd.111.039412
This article has not been copyedited and formatted. The final version may differ from this version.

compound with emphasis on the potential formation of reactive metabolites. The metabolism of rimonabant in RLM incubations has been reported previously (Zhang et al., 2005a). In the present study, masses of metabolites detected were consistent with the literature report. Three major metabolites were detected in both HLMs and RLMs, *N*-aminopiperidine **M1**, the monooxygenated metabolite **M3** (+16 Da) and the dehydrogenated metabolite **M7** (-2 Da) (Scheme 2). **M1** was not reported by Zhang et al, but is a known metabolite of rimonabant (EMEA, 2006). Minor metabolites detected were **M6** (+16 Da, RLMs and HLMs) and **M2**, **M4**, **M5** and **M8** (all +14 Da, HLMs only) (Scheme 2). MSMS spectral analysis indicates that **M2**-**M8** are formed via oxidation of the piperidinyl moiety of rimonabant, as their MSMS spectra contained the unmodified fragment ion at *m/z* 362.99 (**i**$^+$, Scheme 3). This fragment is formed via cleavage of the amide bond and is also the base peak in the MSMS spectrum of rimonabant (Figure 6A). High resolution MSMS spectra of **M3** and **M7** are shown in Figure 6B and C. No additional structural information for **M2** and **M4**-**M6** could be obtained from their MSMS spectra.

To establish the structure of **M3**, its MSMS spectrum was examined (Figure 6B). MSMS spectral analysis of **M3** indicates the loss of water (-18 Da) resulting in a *m/z* 465.0766 fragment ion which, together with the observation of the *m/z* 362.9911 fragment ion, suggests an aliphatic *C*-hydroxylation of the piperidinyl ring. There are three possible structures for **M3**: the 2-, 3- or 4-hydroxypiperidinyl regioisomers (Scheme 4). Dehydrative fragmentation of these hydroxypiperidines may give three isobaric fragment ions at *m/z* 465.0766: 1,2-dehydro-, 2,3-dehydro- and 3,4-dehydropiperidine (Scheme 4). Two additional fragment ions at *m/z* 435.0328 and *m/z* 409.0262 were observed in the MSMS spectrum of **M3** but not from rimonabant. The formation of these fragment ions can be rationalized by further fragmentation of the dehydrogenated fragment at *m/z* 465.0766 via pericyclic mechanisms (Scheme 4). When examining the potential fragmentation products of the different dehydro

species, only the 2,3-dehydropiperidinyl isomer resulting from either the 2- or the 3-hydroxypiperidinyl moiety may form the fragment ions at *m/z* 435.0328 and *m/z* 409.0262. Dehydration of the 2-hydroxypiperidinyl isomer may also lead to the formation of the 1,2-dehydro piperidinyl species, but no secondary fragments from this species are observed in the MSMS spectra of **M3**. Based on this analysis, the major hydroxylated metabolite **M3** of rimonabant is proposed to be the 3-hydroxypiperidinyl species.

To establish the structure of the second major metabolite **M7**, its MSMS spectrum was also examined (Figure 6C). This spectrum reveals that **M7** is formed via dehydrogenation of the piperidinyl ring since the *m/z* 362.99 fragment is present (**M7iv**$^+$, Figure 6C and Scheme 5). The fragment ions observed with **M3H**$^+$ at *m/z* 435.0328 and *m/z* 409.0262 from the pericyclic rearrangements of the 2,3- and 3,4-dehydro-piperidinyl species are absent in the MSMS spectrum of **M7**. Therefore the double bond present in **M7** must be located at the 1,2-position corresponding to the iminium ion **M7H**$^+$. Fragmentation of this iminium species via pericyclic rearrangement is expected to lead to fragment ions at *m/z* 407.0109 and 437.0461 (Scheme 4). However, no such fragments are observed from **M7H**$^+$. Instead, two fragments at *m/z* 422.0685 and *m/z* 447.0650, corresponding to loss of isocyanate and water, respectively, are observed. These fragments are suggested to be formed via intramolecular rearrangements in which the electrophilic iminium ion first is attacked by a lone electron pair of the neighbouring nitrogen on the pyrazole ring or the oxygen of the carbonyl group, respectively (Scheme 5). **M7** is therefore postulated to be the iminium ion metabolite of rimonabant. This is supported by the identification of cyanide adducts in HLM incubations supplemented with KCN. **M7** was nearly completely consumed in the KCN incubations and a major cyanide conjugate **CA2** at *m/z* 492.0854 was detected (Figure 2C). The MSMS spectrum of **CA2** displays a large fragment ion at *m/z* 465.0752 that is formed via loss of hydrogen cyanide

DMD Fast Forward. Published on July 6, 2011 as DOI: 10.1124/dmd.111.039412
This article has not been copyedited and formatted. The final version may differ from this version.

(data not shown). Comparison of MS^3 data of the *m/z* 465.08 fragments formed from **CA2** and **M3** (data not shown) with the MSMS spectrum of $\mathbf{M7H^+}$ reveals that the spectra from **CA2** and **M7** are virtually identical and significantly different from that of **M3**. This shows that **CA2**, but not **M3**, forms the iminium ion (**M7**) upon collision-induced fragmentation.

Zhang et al. proposed that the major rimonabant metabolites, denoted **M3** and **M7** in the present study, are the 2-hydroxypiperidinyl metabolite (an α-carbinolamine) and the 2,3- or 3,4-dehydropiperidinyl species. These conclusions are not supported by our results. We propose that **M3** is the 3-hydroxypiperidinyl metabolite and **M7** the 1,2-dehydropiperidinyl species. Zhang et al.'s suggestion for **M3** is an α-carbinolamine. This system is generally unstable and undergoes cleavage to give the corresponding amine and aldehyde (or in the case of cyclic α-carbinolamines, to give the corresponding aminoaldehyde as shown in Scheme 1) that may be metabolized further to the carboxylic acid and/or alcohol as stable end products. No such cleavage products were observed in our study. In addition, we could find no evidence of methoxylamine-trapped aldehyde intermediates in the methoxylamine supplemented incubations. It is possible, but not likely, that the second +16 Da metabolite **M6** is the 2-hydroxypiperidinyl metabolite. Unfortunately, the MSMS spectrum of **M6** did not reveal the position of the hydroxy group on the piperidinyl ring. However, based on the instability of α-carbinolamines, **M6** is suggested to be the 4-hydroxypiperidinyl metabolite of rimonabant (Scheme 2). Moreover, the identification of **M7** as a reactive iminium ion (the 1,2-dehydropiperidinyl species) is supported by the depletion of **M7** by cyanide and the formation of large amounts of the corresponding cyano adduct **CA2**. However, it should be noted that the 2,3-dehydropiperidinyl species suggested by Zhang et al. is the conjugate base of the iminium ion.

DMD Fast Forward. Published on July 6, 2011 as DOI: 10.1124/dmd.111.039412
This article has not been copyedited and formatted. The final version may differ from this version.

In our study, a high level of covalent binding of rimonabant in incubations with HLMs was observed. It is especially noteworthy that as much as 19% of the metabolic turnover resulted in covalent binding. A majority of the binding can likely be attributed to reactive iminium ion metabolites, as the covalent binding was significantly decreased in incubations with KCN. This was further confirmed by detection of the three cyanide adducts **CA1**-**CA3**, which together accounted for more than 60% of the metabolites formed from rimonabant in KCN supplemented HLM incubations. In incubations with methoxylamine, the covalent binding of rimonabant was also decreased, but to a lesser extent. The obvious possibility for this decrease would be trapping of a reactive aldehyde intermediate, however no such adduct was observed. It is possible that methoxylamine prevents the covalent binding by forming short-lived adducts. This has previously been suggested to occur in covalent binding studies with rosiglitazone and GSH, where a reduction of covalent binding was seen in the presence of GSH, but no adducts could be detected (Usui et al., 2009). **M1** (N-aminopiperidine) was not considered to be a potential contributor to the covalent binding of rimonabant since it does not have any electrophilic structural features. **M1** is, however, a known mutagen (Zeiger and Guthrie, 1981). In the presence of S9, its mutagenicity decreases in the Ames test indicating that its mutagenic action is not metabolism dependent (Zeiger and Guthrie, 1981).

Rimonabant was also found to irreversibly inhibit CYP3A4, which is likely due to covalent binding of rimonabant to its active site. In contrast to this result, the European Public Assessment Report for Acomplia® states that in vitro studies on rimonabant suggest a low potential for inhibition of P450 isoenzymes (EMEA, 2006). From a drug-drug interaction perspective, the TDI of CYP3A4 by rimonabant does not seem important as no effect of rimonabant (40 mg once daily for 8 days) on the pharmacokinetics of the CYP3A4 substrate midazolam (0.03 mg/kg single oral dose) could be observed in a clinical study (EMEA,

2006). However, many drugs exhibiting TDI are also associated with (I)ADRs suggesting that TDI is not only an indicator of potential drug-drug interactions, but also of idiosyncratic toxicity (Riley et al., 2007).

In conclusion, our studies on the *in vitro* metabolism of rimonabant clearly show the formation of reactive intermediates that irreversibly bind to hepatic proteins to a significant extent and metabolism-dependent irreversible inhibition of CYP3A4. Nonetheless, in contrast to the findings presented in the current study, to date no toxicities obviously related to the formation of reactive metabolites from rimonabant have been reported. Recently, it was suggested that a better prediction of ADRs can be achieved by evaluating covalent binding values together with the daily dose of the drug (Obach et al., 2008; Bauman et al., 2009; Nakayama et al., 2009; Usui et al., 2009; Thompson et al., 2010). Despite the high extent of covalent binding observed with rimonabant, the low recommended dose (20 mg) for this particular drug might have limited the occurrence of ADRs that could be attributable to reactive metabolites.

Acknowledgements

We thank Anna-Pia Palmgren for performing the TDI experiments and the AstraZeneca radiochemistry team in Mölndal for supplying the radiolabelled test compound. We also thank Dr. Lars Weidolf for helpful discussions and constructive reading of the manuscript.

Authorship Contributions:

Participated in research design: Andresen Bergström, Isin, Castagnoli and Milne

Conducted experiments: Andresen Bergström

Performed data analysis: Andresen Bergström, Isin, Castagnoli and Milne

Wrote or contributed to the writing of the manuscript: Andresen Bergström, Isin, Castagnoli and Milne

References

Argoti D, Liang L, Conteh A, Chen L, Bershas D, Yu C-P, Vouros P and Yang E (2005) Cyanide trapping of iminium ion reactive intermediates followed by detection and structure identification using liquid chromatography-tandem mass spectrometry (LC-MS/MS). *Chem. Res. Toxicol.* 18:1537-1544.

Atkinson A, Kenny JR and Grime K (2005) Automated assessment of time-dependent inhibition of human cytochrome P450 enzymes using liquid chromatography-tandem mass spectrometry analysis. *Drug. Metab. Dispos.* 33:1637-1647.

Avent KM, DeVoss JJ and Gillam EM (2006) Cytochrome P450-mediated metabolism of haloperidol and reduced haloperidol to pyridinium metabolites. *Chem. Res. Toxicol.* 19:914-920.

Baillie TA (2008) Metabolism and toxicity of drugs. Two decades of progress in industrial drug metabolism. *Chem. Res. Toxicol.* 21:129-137.

Bauman JN, Kelly JM, Tripathy S, Zhao SX, Lam WW, Kalgutkar AS and Obach RS (2009) Can in vitro metabolism-dependent covalent binding data distinguish hepatotoxic from nonhepatotoxic drugs? An analysis using human hepatocytes and liver S-9 fraction. *Chem. Res. Toxicol.* 22:332-340.

Boyd ST and Fremming BA (2005) Rimonabant-a selective CB1 antagonist. *Ann. Pharmacother.* 39:684-690.

Castagnoli N, Jr., Rimoldi JM, Bloomquist J and Castagnoli KP (1997) Potential metabolic bioactivation pathways involving cyclic tertiary amines and azaarenes. *Chem. Res. Toxicol.* 10:924-940.

Christensen R., Kristensen PK, Bartels, EM, Bliddal H, Astrup, A (2007) Efficacy and safety of the weight-loss drug rimonabant: a meta analysis of randomised trials. *Lancet* 370:1706-1713.

Dalton GD, Bass CE, Van Horn CG and Howlett AC (2009) Signal transduction via cannabinoid receptors. *CNS Neurol. Disord.-Dr.* 8:422-431.

Dalvie DK and O'Connell TN (2004) Characterization of novel dihydrothienopyridinium and thienopyridinium metabolites of ticlopidine in vitro: role of peroxidases, cytochromes p450, and monoamine oxidases. *Drug. Metab. Dispos.* 32:49-57.

Di Marzo V (2009) The endocannabinoid system: its general strategy of action, tools for its pharmacological manipulation and potential therapeutic exploitation. *Pharmacol. Res.* 60:77-84.

EMEA (2006) Acomplia: European Public Assessment Report. Scientific Discussion. Available from http://www.ema.europa.eu/ema/index.jsp?curl=pages/medicines/human/medicines/000666/human_med_000623.jsp&murl=menus/medicines/medicines.jsp&mid=WC0b01ac058001d125 [Accessed 2011 March 10].

Evans DC, Watt AP, Nicoll-Griffith DA and Baillie TA (2004) Drug-protein adducts: An industry perspective on minimizing the potential for drug bioactivation in drug discovery and development. *Chem. Res. Toxicol.* 17:3-16.

Franklin MR (1991) Cytochrome P450 metabolic intermediate complexes from macrolide antibiotics and related compounds. *Methods Enzymol.* 206:559-573.

Grimm SW, Einolf HJ, Hall SD, He K, Lim HK, Ling KH, Lu C, Nomeir AA, Seibert E, Skordos KW, Tonn GR, Van Horn R, Wang RW, Wong YN, Yang TJ and Obach RS (2009) The conduct of in vitro studies to address time-dependent inhibition of drug-metabolizing enzymes: a perspective of the pharmaceutical research and manufacturers of America. *Drug. Metab. Dispos.* 37:1355-1370.

Guengerich FP and MacDonald JS (2007) Applying mechanisms of chemical toxicity to predict drug safety. *Chem. Res. Toxicol.* 20:344-369.

Henness S, Robinson DM and Lyseng-Williamson KA (2006) Rimonabant. *Drugs* 66:2109-2119; discussion 2120-2101.

Howlett AC, Barth F, Bonner TI, Cabral G, Casellas P, Devane WA, Felder CC, Herkenham M, Mackie K, Martin BR, Mechoulam R and Pertwee RG (2002) International Union of Pharmacology. XXVII. Classification of cannabinoid receptors. *Pharmacol. Rev.* 54:161-202.

Kalgutkar AS and Soglia JR (2005) Minimising the potential for metabolic activation in drug discovery. *Expert Opin. Drug Metab. Toxicol.* 1:91-142.

Markwell MAK, Haas SM, Bieber LL and Tolbert NE (1978) A modification of the Lowry procedure to simplify protein determination in membrane and lipoprotein samples. *Anal. Biochem.* 87:207-210.

Masic LP (2011) Role of cyclic tertiary amine bioactivation to reactive iminium species: structure toxicity relationship. *Curr. Drug Metab.* 12:35-50.

Murphy PJ (1973) Enzymatic oxidation of nicotine to nicotine 1'(5') iminium ion. A newly discovered intermediate in the metabolism of nicotine. *J. Biol. Chem.* 248:2796-2800.

Nakayama S, Atsumi R, Takakusa H, Kobayashi Y, Kurihara A, Nagai Y, Nakai D and Okazaki O (2009) A zone classification system for risk assessment of idiosyncratic drug toxicity using daily dose and covalent binding. *Drug Metab. Dispos.* 37:1970-1977.

Obach RS, Kalgutkar AS, Soglia JR and Zhao SX (2008) Can in vitro metabolism-dependent covalent binding data in liver microsomes distinguish hepatotoxic from nonhepatotoxic drugs? An analysis of 18 drugs with consideration of intrinsic clearance and daily dose. *Chem. Res. Toxicol.* 21:1814-1822.

Obach RS and Van Vunakis H (1988) Non-metabolic covalent binding of nicotine-delta 1'(5')-iminium ion to liver microsomes and sulfhydryl-containing polyamino acids. *Biochem. Pharmacol.* 37:4601-4604.

Owens SM, Gunnell M, Laurenzana EM and Valentine JL (1993) Dose- and time-dependent changes in phencyclidine metabolite covalent binding in rats and the possible role of CYP2D1. *J. Pharmacol. Exp. Ther.* 265:1261-1266.

Pertwee RG (2006) Cannabinoid pharmacology: the first 66 years. *Brit. J. Pharmacol.* 147 Suppl 1:S163-171.

Polasek TM and Miners JO (2007) In vitro approaches to investigate mechanism-based inactivation of CYP enzymes. *Expert Opin. Drug Metab. Toxicol.* 3:321-329.

Riley RJ, Grime K and Weaver R (2007) Time-dependent CYP inhibition. *Expert Opin. Drug Metab. Toxicol.* 3:51-66.

Sayre LM, Engelhart DA, Nadkarni DV, Manoj Babu MK, Flammang AM and McCoy GD (1997) The role of iminium-enamine species in the toxication and detoxication of cyclic tertiary amines. *NIDA Res. Monogr.* 173:106-127.

Shenton JM, Chen J and Uetrecht JP (2004) Animal models of idiosyncratic drug reactions. *Chem.-Biol. Interact.* 150:53-70.

Shigenaga MK, Trevor AJ and Castagnoli N, Jr. (1988) Metabolism-dependent covalent binding of (S)-[5-3H]nicotine to liver and lung microsomal macromolecules. *Drug Metab. Dispos.* 16:397-402.

Thompson RA, Isin EM, Li Y, Weaver R, Weidolf L, Wilson I, Claesson A, Page K, Dolgos H and Kenna JG (2011) Risk assessment and mitigation strategies for reactive metabolites in drug discovery and development. *Chem. Biol. Interact.*192:65-71.

Uetrecht J (2008) Idiosyncratic drug reactions: past, present, and future. *Chem. Res. Toxicol.* 21:84-92.

Usui T, Mise M, Hashizume T, Yabuki M and Komuro S (2009) Evaluation of the potential for drug-induced liver injury based on in vitro covalent binding to human liver proteins. *Drug. Metab. Dispos.* 37:2383-2392.

Van Gaal LF, Rissanen AM, Scheen AJ, Ziegler O, Rossner S and Group RI-ES (2005) Effects of the cannabinoid-1 receptor blocker rimonabant on weight reduction and cardiovascular risk factors in overweight patients: 1-year experience from the RIO-Europe study. *Lancet* 365:1389-1397.

Ward DP, Trevor AJ, Kalir A, Adams JD, Baillie TA and Castagnoli N, Jr. (1982) Metabolism of phencyclidine. The role of iminium ion formation in covalent binding to rabbit microsomal protein. *Drug Metab. Dispos.* 10:690-695.

Zeiger E and Guthrie J (1981) Cyclic hydrazides are mutagenic for Salmonella typhimurium. *Mutat. Res.* 91:199-205.

Zhang Q, Ma P, Wang W, Cole RB and Wang G (2005a) In vitro metabolism of diarylpyrazoles, a novel group of cannabinoid receptor ligands. *Drug Metab. Dispos.* 33:508-517.

Zhang Z, Chen Q, Li Y, Doss GA, Dean BJ, Ngui JS, Silva Elipe M, Kim S, Wu JY, Dininno F, Hammond ML, Stearns RA, Evans DC, Baillie TA and Tang W (2005b) In vitro bioactivation of dihydrobenzoxathiin selective estrogen receptor modulators by cytochrome P450 3A4 in human liver microsomes: formation of reactive iminium and quinone type metabolites. *Chem. Res. Toxicol.* 18:675-685.

DMD Fast Forward. Published on July 6, 2011 as DOI: 10.1124/dmd.111.039412
This article has not been copyedited and formatted. The final version may differ from this version.

Legends for Figures

Figure 1. Rimonabant

Figure 2. LC-RAD metabolite profiles of [^{14}C]rimonabant after 60 min incubation with human liver microsomes (A), rat liver microsomes (B) and human liver microsomes supplemented with 1 mM KCN (C).

Figure 3. Covalent binding of [^{14}C]rimonabant in incubations with and without trapping agents. The covalent binding values have been corrected for the %conversion of parent.

Figure 4. Time-dependent inhibition of recombinant CYP3A4 by rimonabant, troleandomycin (positive control) and betamethasone (negative control). The results are expressed as the normalized ratio of the metabolic activity of inhibited incubations versus non-inhibited incubations.

Figure 5. Ferricyanide displacement of inhibited recombinant CYP3A4. Rimonabant and troleandomycin (positive control) were used as inhibitors. The results are expressed as the normalized ratio of the metabolic activity of inhibited incubations versus non-inhibited incubations.

Figure 6. MSMS spectra of (A) rimonabant, (B) **M3**, (C) **M7**.

Table 1. Quantitative Estimates (% of Total Radioactivity) of Rimonabant, Metabolites and Trapped Adducts in Incubates[a] from Human and Rat Liver Microsomal Incubations

compound	retention time (min)	observed m/z	proposed composition	error (ppm)	mass shift[b]	transformation	% of total radioactivity in incubate				
							HLMs no trapping agent	RLMs no trapping agent	HLMs cyanide	HLMs gluta-thione	HLMs methoxyl-amine
M1	1.7				-362 Da	$-C_{17}H_{10}Cl_3N_2O$	5.3	6.0	2.9	9.8	2.4
M2	10.4	481.0708	$C_{20}{}^{14}C_2H_{20}Cl_3N_4O_2$	1.9	+14 Da	+O -2H	0.9	-	-	0.5	0.4
M3	11.7	483.0852	$C_{20}{}^{14}C_2H_{22}Cl_3N_4O_2$	4.3	+16 Da	+O	6.7	7.7	5.6	6.9	2.6
M4	12.0	481.0712	$C_{20}{}^{14}C_2H_{20}Cl_3N_4O_2$	1.0	+14 Da	+O -2H	0.6	-	-	-	1.0
M5	13.2	481.0726	$C_{20}{}^{14}C_2H_{20}Cl_3N_4O_2$	1.9	+14 Da	+O -2H	0.9	-	0.3	0.8	-
M6	14.2	483.0870	$C_{20}{}^{14}C_2H_{22}Cl_3N_4O_2$	0.6	+16 Da	+O	0.3	0.8	0.5	0.5	0.4
CA1	15.1	508.0802	$C_{21}{}^{14}C_2H_{21}Cl_3N_5O_2$	4.7	+41 Da	+O +CN -H	-	-	0.8	-	-
M7, M8[c]	17.3	465.0753	$C_{20}{}^{14}C_2H_{20}Cl_3N_4O$	3.2	-2 Da,	-2H,	24.6[d]	5.6[d]	2.5[d]	26.2[d]	8.9[d]
		481.0707	$C_{20}{}^{14}C_2H_{20}Cl_3N_4O_2$	2.1	+14 Da	+O -2H					
rimonabant	23.2	467.0887	$C_{20}{}^{14}C_2H_{22}Cl_3N_4O$	7.9	0 Da	Parent	60.7	79.0	67.2	55.0	83.8
CA2	24.4	492.0853	$C_{21}{}^{14}C_2H_{21}Cl_3N_5O$	4.9	+25 Da	+CN -H	-	-	18.0	-	-
CA3	27.1	490.0690	$C_{21}{}^{14}C_2H_{19}Cl_3N_5O$	6.3	+23 Da	+CN -3H	-	-	1.3	-	-

[a] measured in pooled incubates (n=3).

[b] difference in mass compared to parent. Determined by MS detection for all metabolites and adducts except **M1**, which was identified using comparison of retention time with a synthetic standard.

[c] co-eluting metabolites resolved by differences in masses.

[d] the ratio of **M7**/**M8** measured by MS detection assuming equal response in HLM incubations was *ca* 99:1 with no trapping agent and in the presence of glutathione or methoxylamine and 27:73 in the presence of cyanide. **M8** was not detected in RLM incubations.

- not detected.

Table 2. Covalent Binding and Metabolic Conversion of [^{14}C]Rimonabant in Human Liver Microsomal Incubations With and Without Reactive Metabolite Trappers

test compound	trapper	NADPH (yes/no)	covalent binding ±SD[a] (pmol eq./mg protein)	conversion[b] (%)	corrected covalent binding[c] (pmol eq./mg protein)	Fraction covalent binding[d]
[^{14}C]rimonabant	*no trapper*	yes	920 ±24	49	920	0.19
	no trapper	no	10 ±0.3	NA	NA	NA
	cyanide	yes	432 ±17	37	578	0.12
	glutathione	yes	811 ±59	47	851	0.17
	methoxylamine	yes	182 ±6.1	14	633	0.13

[a] means of 3 incubations ± standard deviation

[b] metabolic conversion of [^{14}C]rimonabant measured by LC-RAD

[c] covalent binding values measured in the incubations with trappers are corrected for the difference in % conversion of parent compared to the no trapper incubation with NADPH. (i.e. corrected covalent binding = (covalent binding in the presence of trapper/conversion in the presence of trapper)*conversion in the absence of trapper)

[d] the fraction covalent binding is calculated as follows:
fCVB = covalent binding × protein concentration / (total radioactivity in incubation × conversion)

NA not applicable

DMD Fast Forward. Published on July 6, 2011 as DOI: 10.1124/dmd.111.039412
This article has not been copyedited and formatted. The final version may differ from this version.

Scheme 1. Equilibrium of the cyclic iminium ion with the corresponding carbinolamine, enamine and aminoaldehyde.

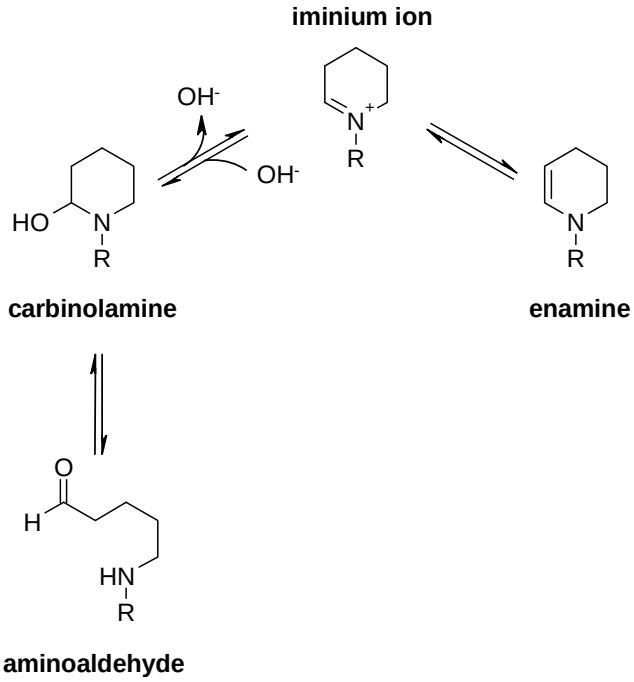

Scheme 2. Proposed biotransformation pathways of rimonabant and cyanide trapping of its metabolites in human liver microsomes.

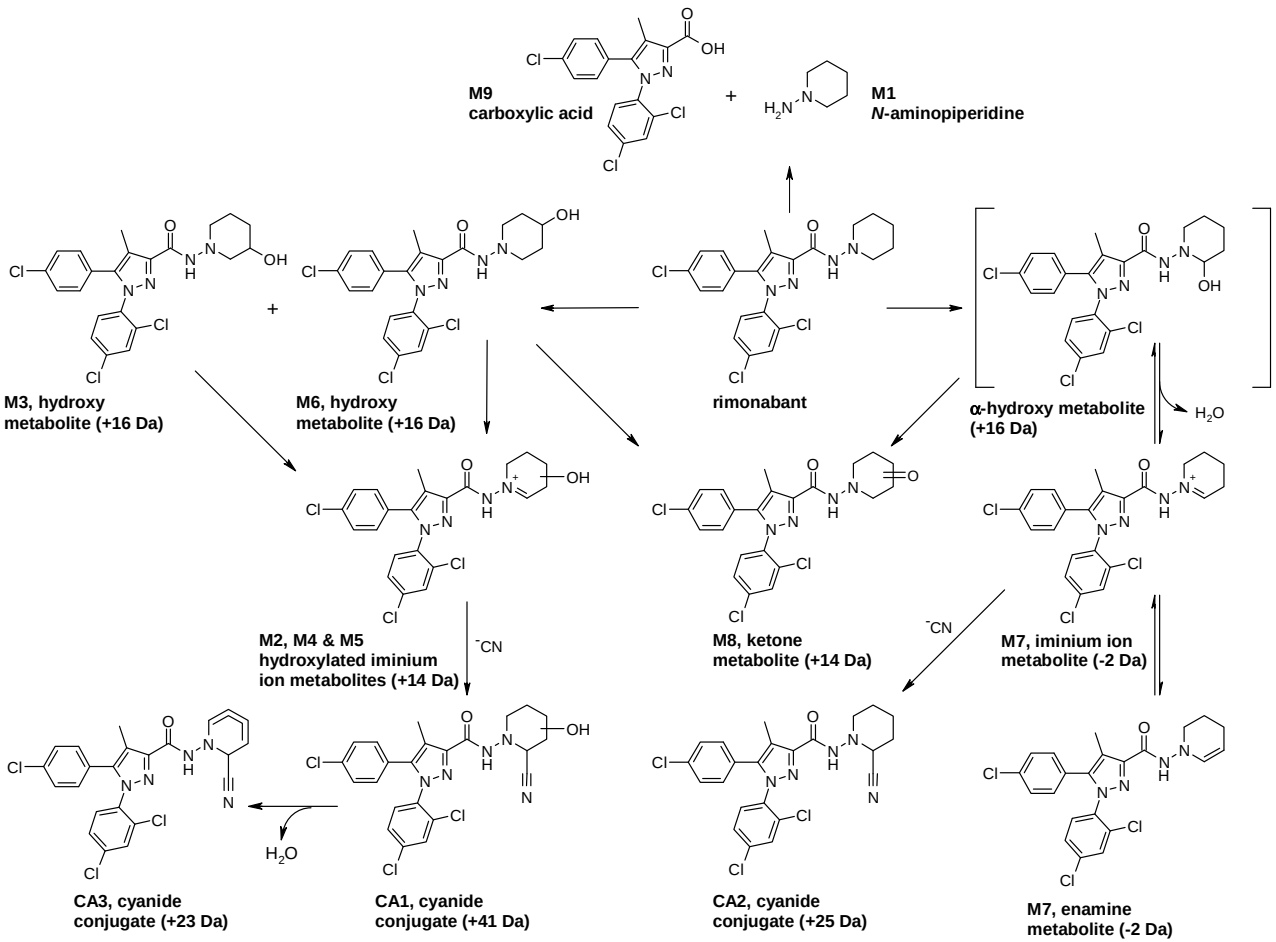

DMD Fast Forward. Published on July 6, 2011 as DOI: 10.1124/dmd.111.039412
This article has not been copyedited and formatted. The final version may differ from this version.

Scheme 3. Formation of the *m/z* 362.99 fragment ion from rimonabant (calculated *m/z* values are shown underneath the structures).

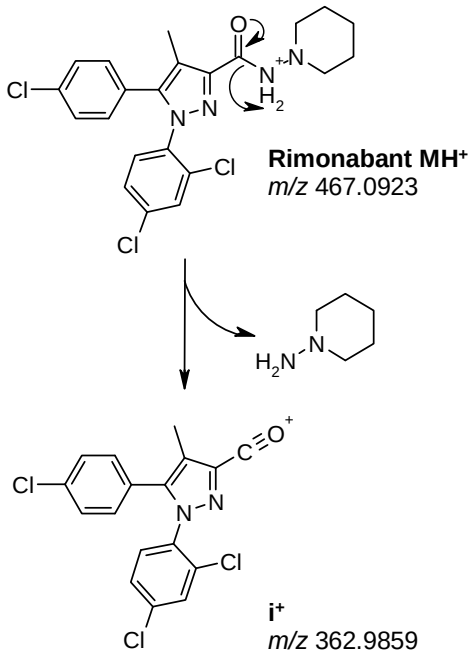

DMD Fast Forward. Published on July 6, 2011 as DOI: 10.1124/dmd.111.039412
This article has not been copyedited and formatted. The final version may differ from this version.

Scheme 4. Collision-induced dehydration of possible hydroxylpiperidinyl metabolites of rimonabant (**M3**) and further fragmentation of dehydro products via pericyclic rearrangement.

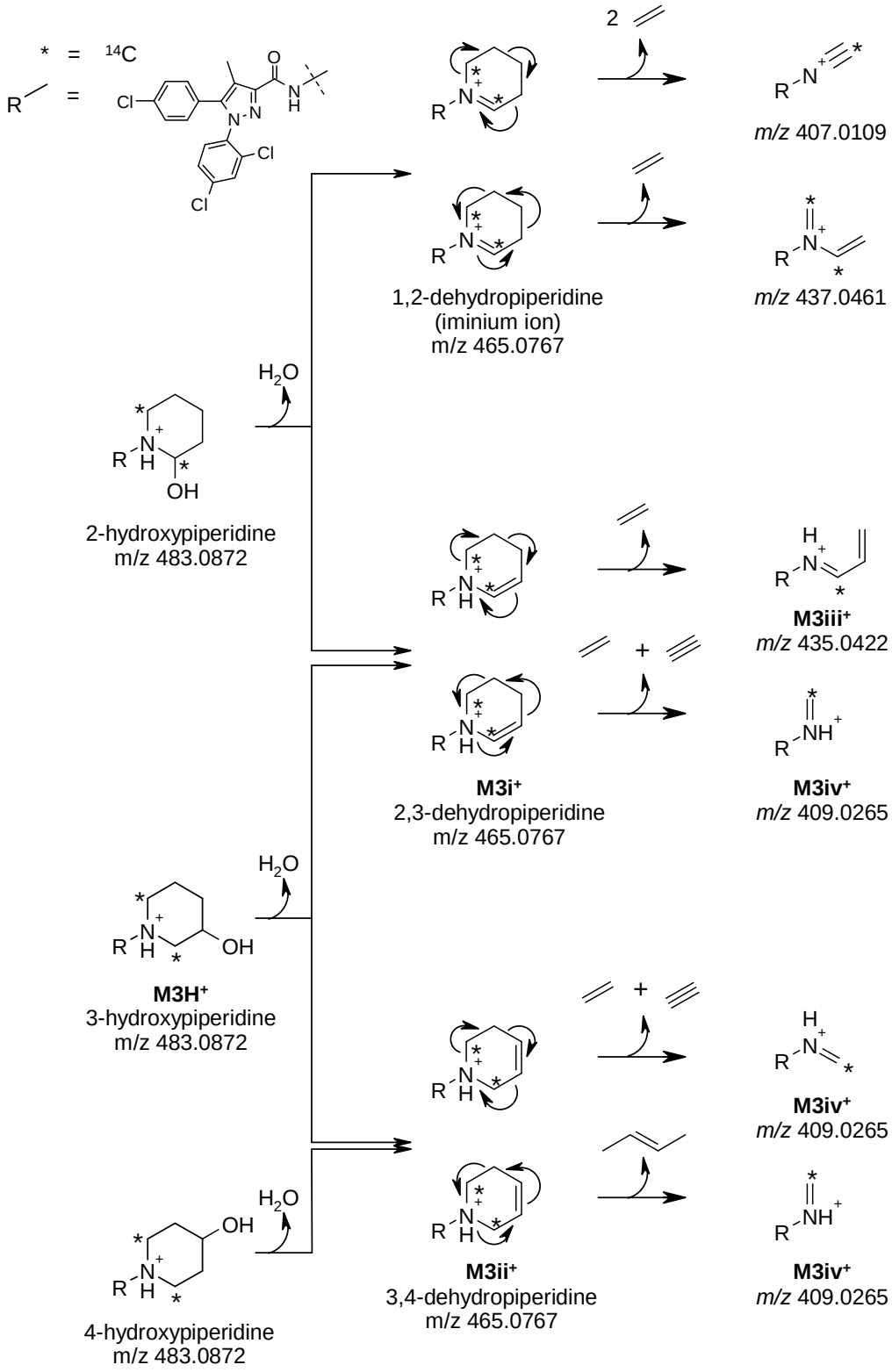

DMD Fast Forward. Published on July 6, 2011 as DOI: 10.1124/dmd.111.039412
This article has not been copyedited and formatted. The final version may differ from this version.

Scheme 5. Proposed MSMS fragmentation pathways of rimonabant metabolite **M7**.

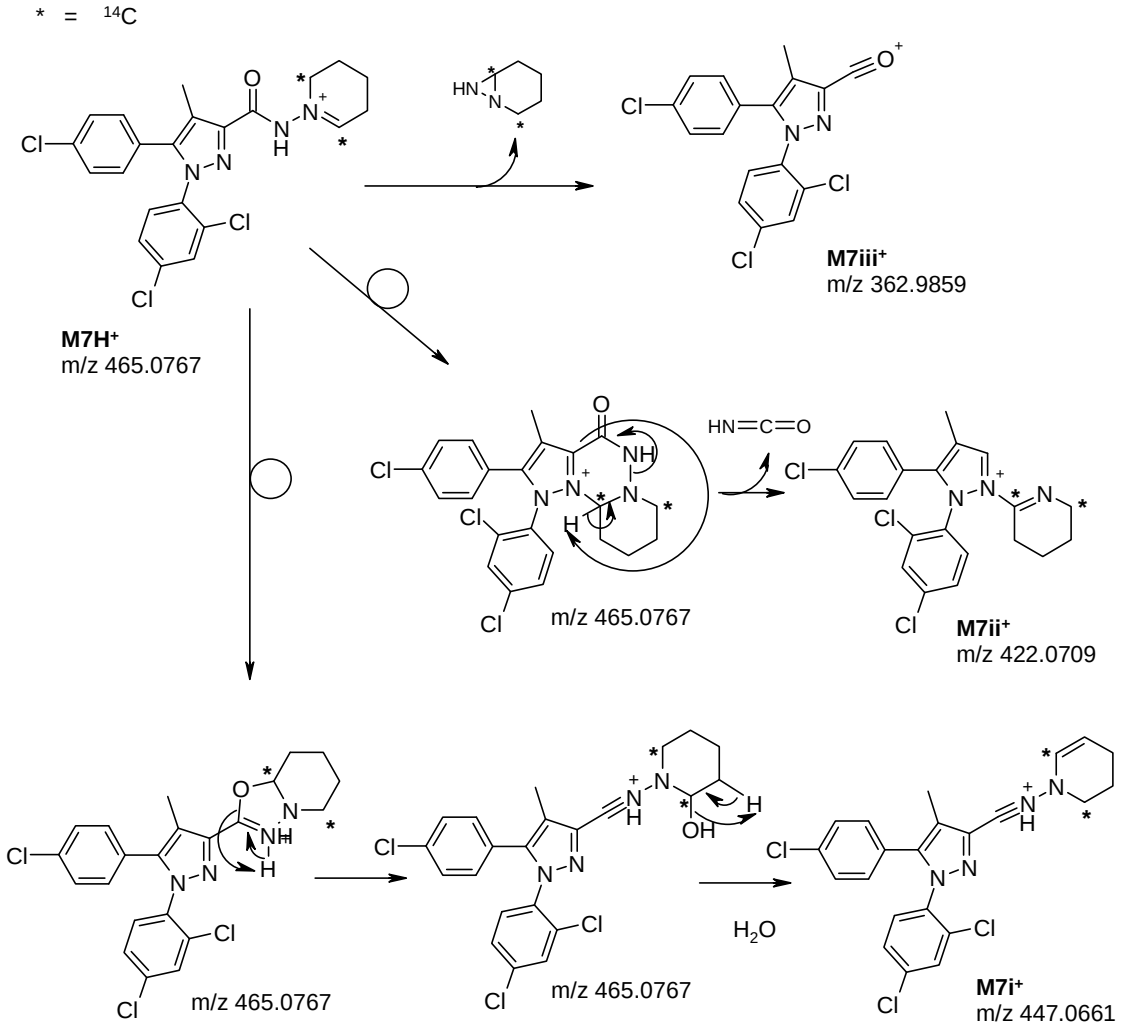

DMD Fast Forward. Published on July 6, 2011 as DOI: 10.1124/dmd.111.039412
This article has not been copyedited and formatted. The final version may differ from this version.

Figure 1

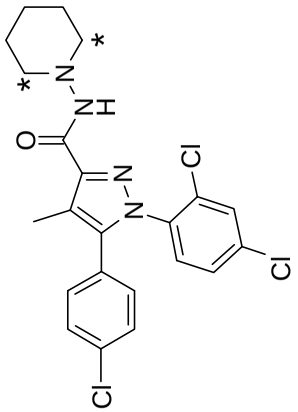

Figure 2

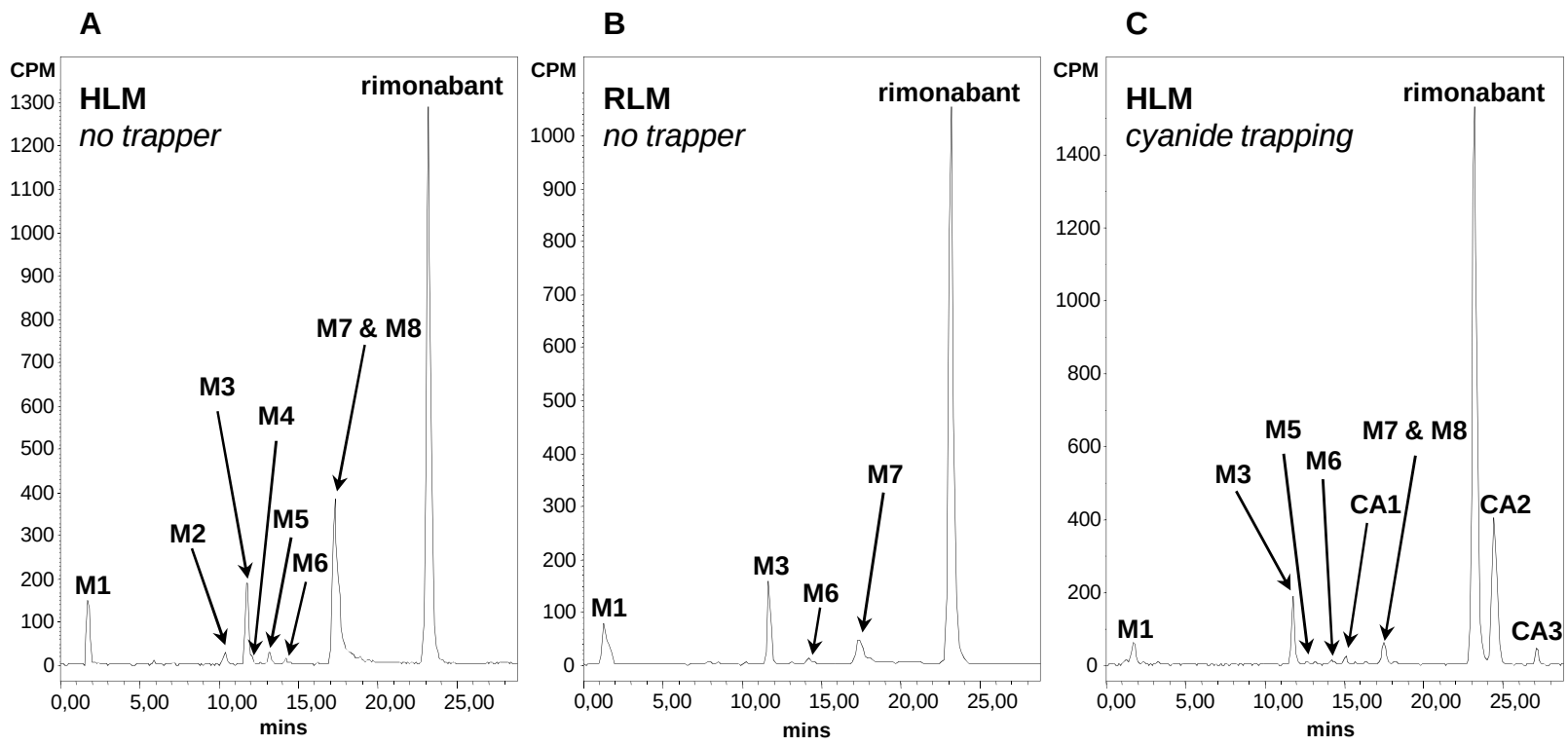

DMD Fast Forward. Published on July 6, 2011 as DOI: 10.1124/dmd.111.039412
This article has not been copyedited and formatted. The final version may differ from this version.

Figure 3

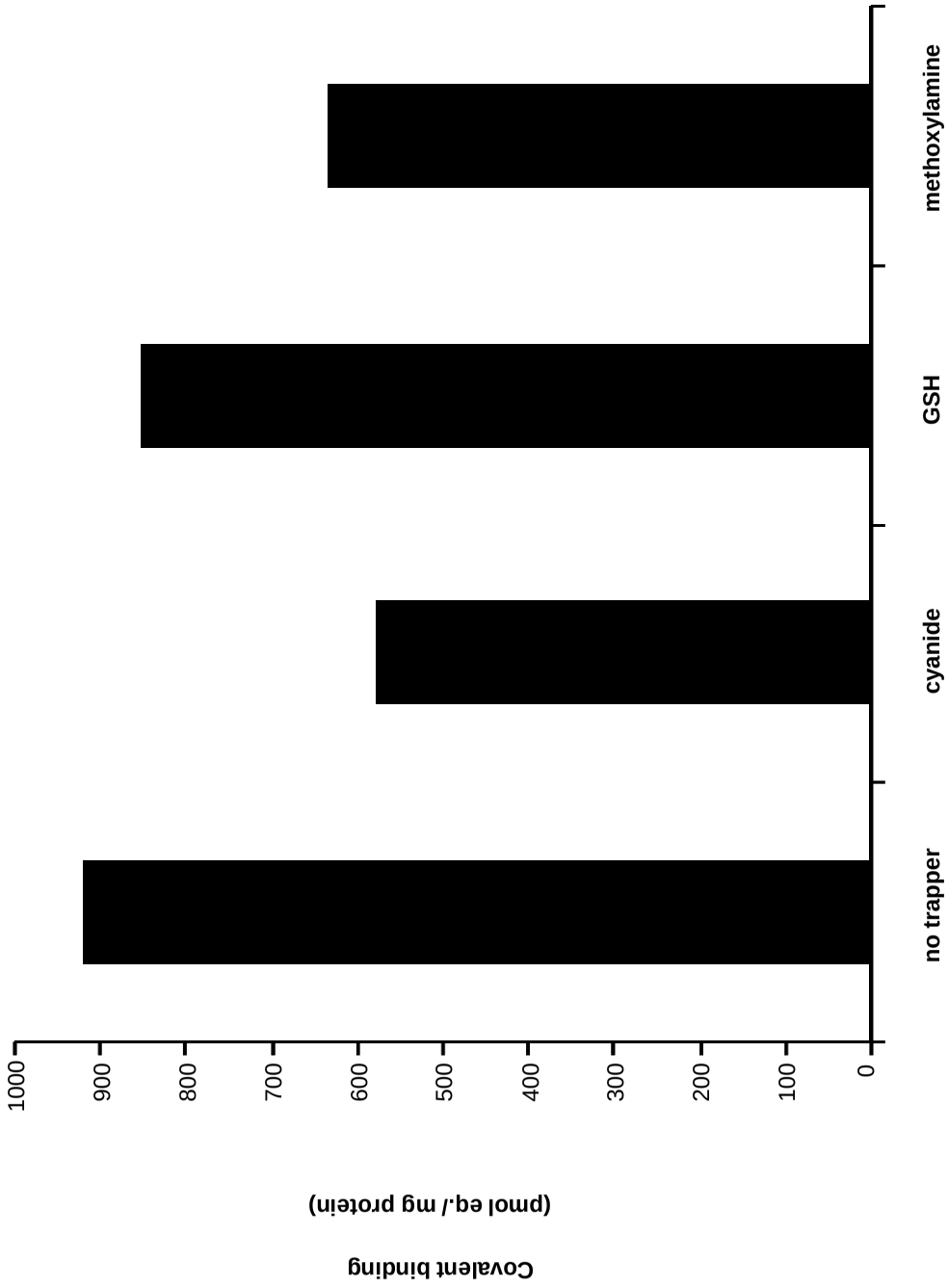

Figure 4

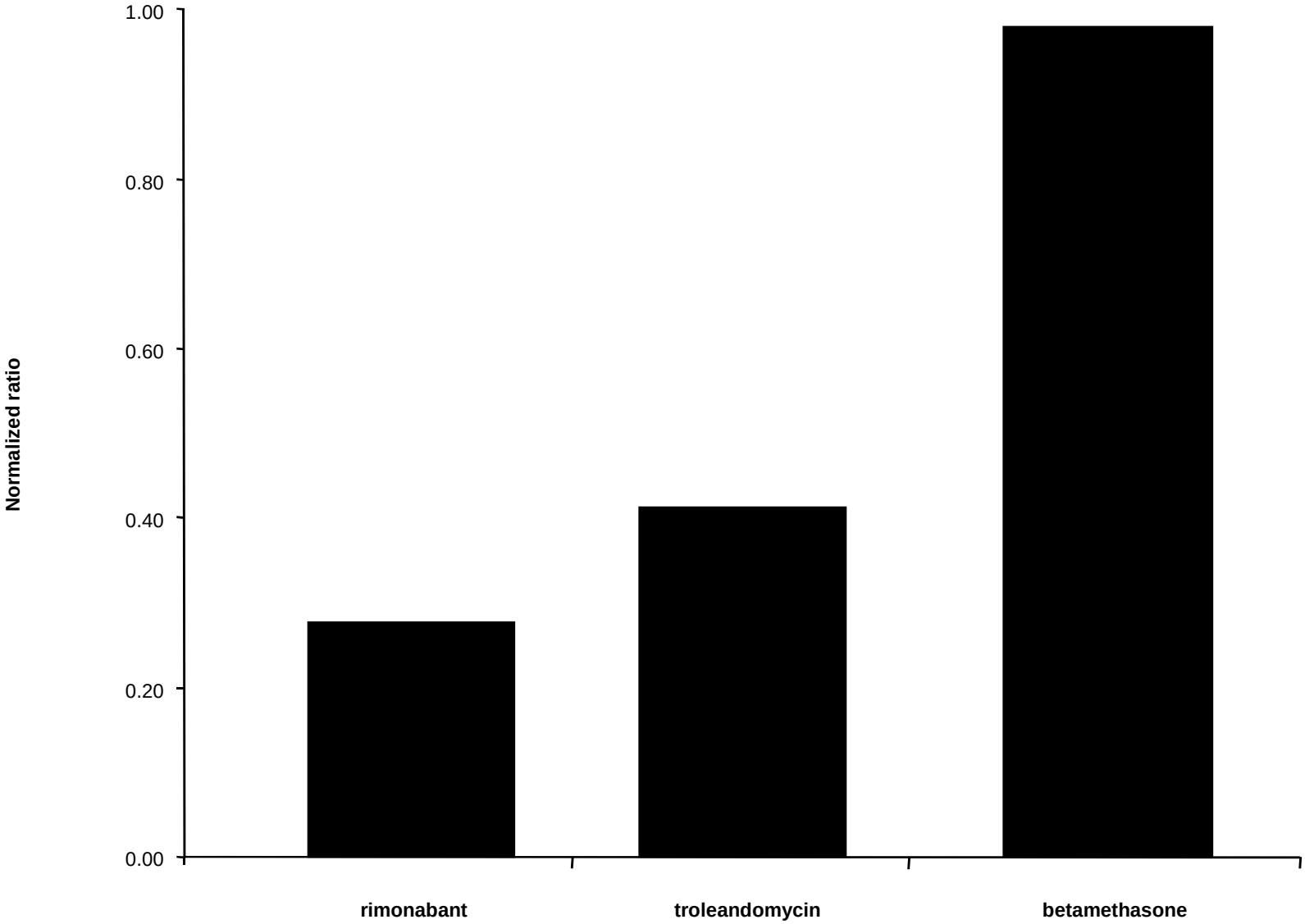

Figure 5

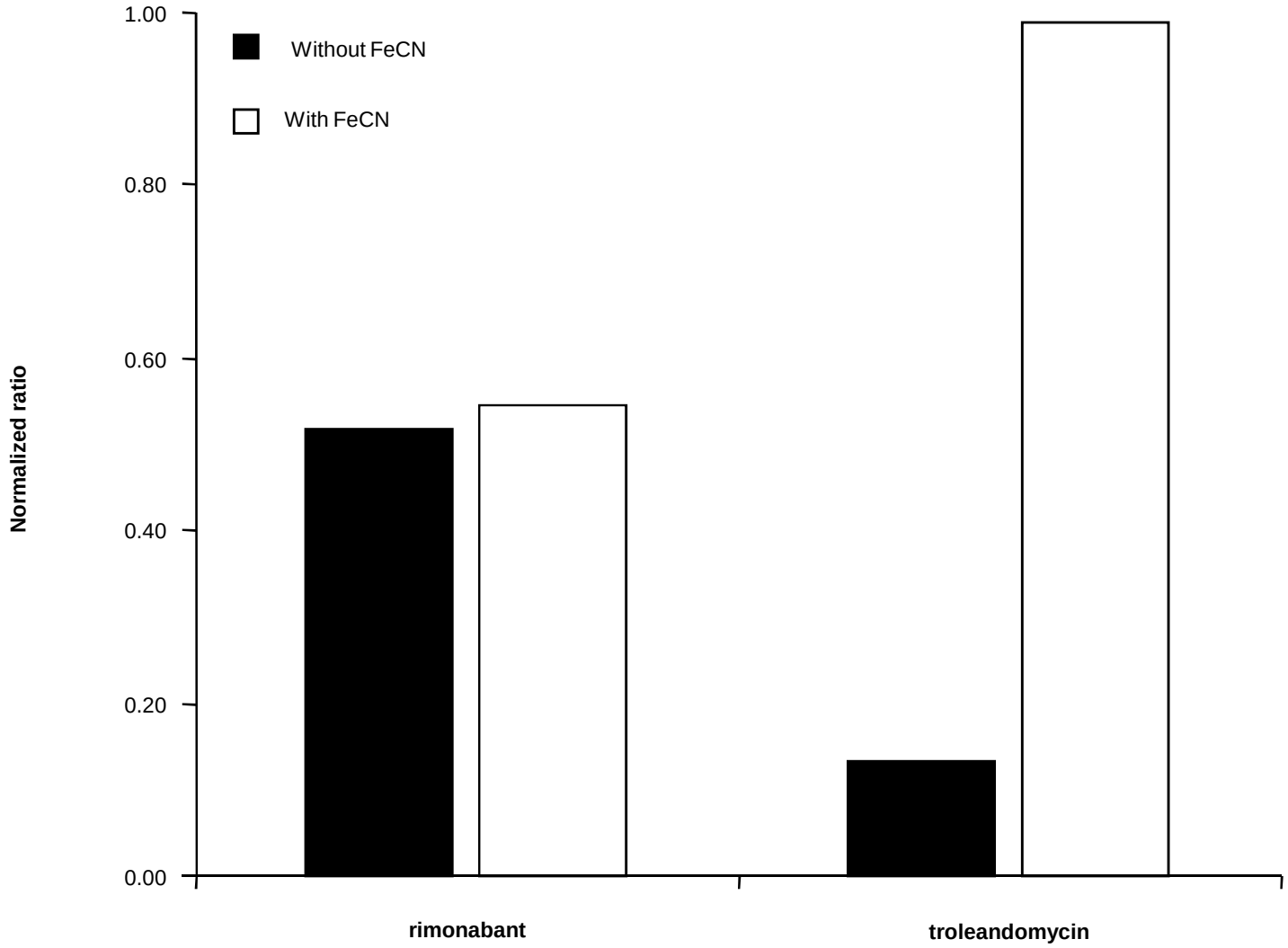

DMD Fast Forward. Published on July 6, 2011 as DOI: 10.1124/dmd.111.039412
This article has not been copyedited and formatted. The final version may differ from this version.

Figure 6

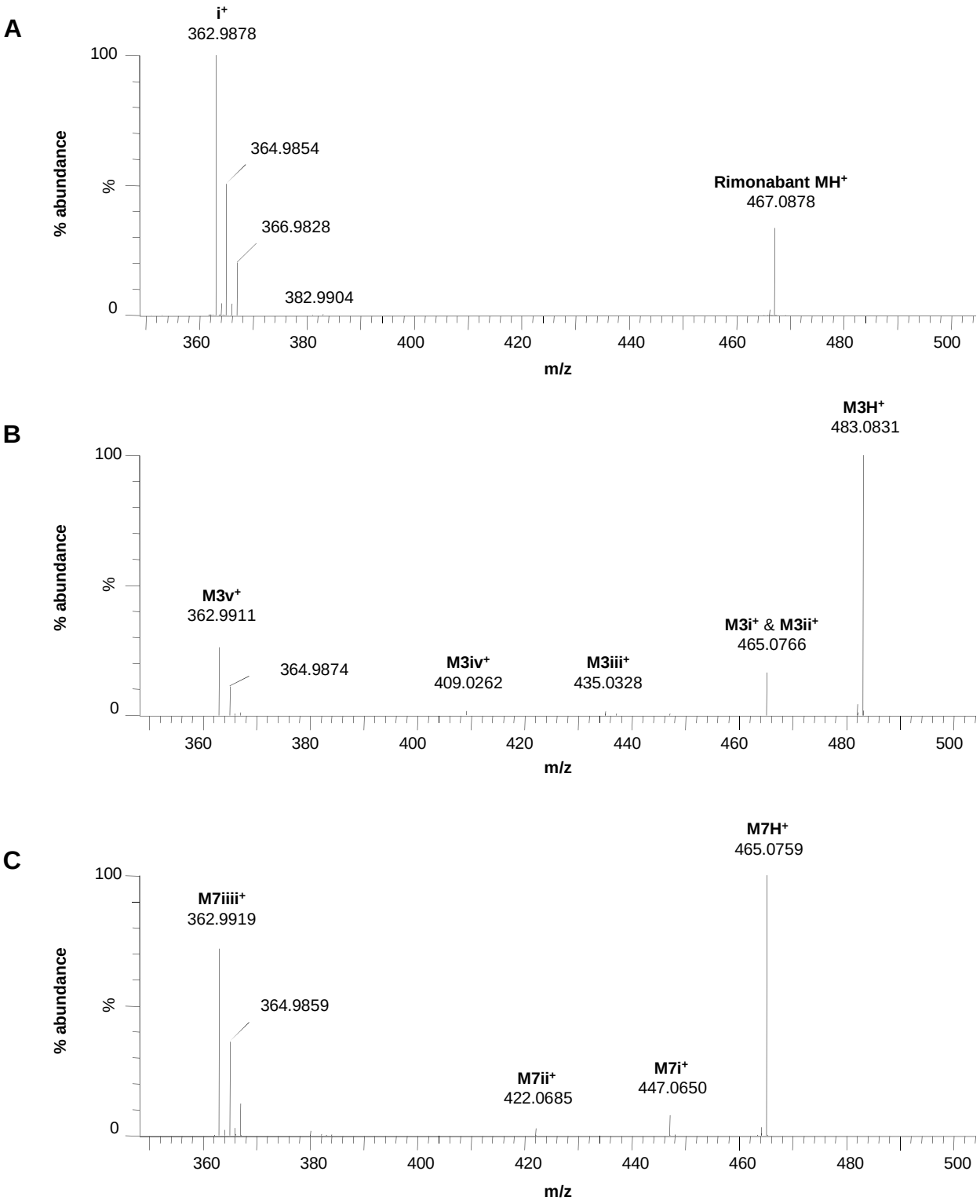

SUPPLEMENTARY INFORMATION

Bioactivation Pathways of the CB1r Antagonist Rimonabant

Moa Andresen Bergström, Emre M. Isin, Neal Castagnoli Jr., and Claire E. Milne

Drug Metabolism and Disposition

Figure 1. Raw data for time dependent inhibition of P450 3A4 by rimonabant